10-15-2009

A Spectroscopically Confirmed Excess of 24 μm Sources in a Super Galaxy Group at z=0.37: Enhanced Dusty Star Formation Relative to the Cluster and Field Environment

Kim-Vy H. Tran
Texas A&M University; University of Zürich

Amelie Saintonge
University of Zürich

John Moustakas
University of California - San Diego

Lei Bai
University of Arizona; Observatories of the Carnegie Institution of Washington

Anthony H. Gonzalez
University of Florida

See next page for additional authors

Authors
Kim-Vy H. Tran, Amelie Saintonge, John Moustakas, Lei Bai, Anthony H. Gonzalez, Bradford P. Holden, Dennis Zaritsky, and Stefan Kautsch

The Astrophysical Journal, 705:809–820, 2009 November 1 doi:10.1088/0004-637X/705/1/809

A SPECTROSCOPICALLY CONFIRMED EXCESS OF 24 μm SOURCES IN A SUPER GALAXY GROUP AT $z = 0.37$: ENHANCED DUSTY STAR FORMATION RELATIVE TO THE CLUSTER AND FIELD ENVIRONMENT

Kim-Vy H. Tran[1,2], Amélie Saintonge[1], John Moustakas[3,4], Lei Bai[5,6], Anthony H. Gonzalez[7], Bradford P. Holden[8], Dennis Zaritsky[5], and Stefan J. Kautsch[7]

[1] Institute for Theoretical Physics, University of Zürich, CH-8057 Zürich, Switzerland
[2] George P. and Cynthia W. Mitchell Institute for Fundamental Physics and Astronomy, Department of Physics, Texas A&M University, College Station, TX 77843, USA; vy@physics.tamu.edu
[3] Center for Cosmology and Particle Physics, 4 Washington Place, New York University, New York, NY 10003, USA
[4] Center for Astrophysics and Space Sciences, University of California, San Diego, 9500 Gilman Drive, La Jolla, CA 92093, USA
[5] Steward Observatory, University of Arizona, 933 North Cherry Avenue, Tucson, AZ 85721, USA
[6] Observatories of the Carnegie Institution of Washington, 813, Santa Barbara Street, Pasadena, CA 91101, USA
[7] Department of Astronomy, University of Florida, Gainesville, FL 32611, USA
[8] UCO/Lick Observatories, University of California, Santa Cruz, CA 95064, USA
Received 2009 July 24; accepted 2009 September 21; published 2009 October 15

ABSTRACT

To trace how dust-obscured star formation varies with environment, we compare the fraction of 24 μm sources in a super galaxy group to the field and a rich galaxy cluster at $z \sim 0.35$. We draw on multi-wavelength observations[9] that combine *Hubble*, *Chandra*, and *Spitzer* imaging with extensive optical spectroscopy (>1800 redshifts) to isolate galaxies in each environment and thus ensure a uniform analysis. We focus on the four galaxy groups ($\sigma_{1D} = 303$–580 km s^{-1}) in supergroup 1120-12 that will merge to form a galaxy cluster comparable in mass to Coma. We find that (1) the fraction of supergroup galaxies with $\mathrm{SFR_{IR}} \geqslant 3\,M_\odot$ yr^{-1} is 4 times higher than in the cluster ($32\% \pm 5\%$ versus $7\% \pm 2\%$); (2) the supergroup's infrared luminosity function confirms that it has a higher density of IR members compared to the cluster and includes bright IR sources ($\log(L_{\mathrm{IR}})[\mathrm{erg\ s^{-1}}] > 45$) not found in galaxy clusters at $z \lesssim 0.35$; and (3) there is a strong trend of decreasing 24 μm fraction with increasing galaxy density, i.e., an infrared–density relation, not observed in the cluster. These dramatic differences are surprising because the early-type fraction in the supergroup is already as high as in clusters, i.e., the timescales for morphological transformation cannot be strongly coupled to when the star formation is completely quenched. The supergroup has a significant fraction ($\sim 17\%$) of luminous, low-mass ($10.0 < \log(M_*)[M_\odot] < 10.6$), $\mathrm{SFR_{IR}} \geqslant 3\,M_\odot$ yr^{-1} members that are outside the group cores ($R_{\mathrm{proj}} \geqslant 0.5$ Mpc); once their star formation is quenched, most will evolve into faint red galaxies. Our analysis indicates that the supergroup's 24 μm population also differs from that in the field: (1) despite the supergroup having twice the fraction of E/S0s as the field, the fraction of $\mathrm{SFR_{IR}} \geqslant 3\,M_\odot$ yr^{-1} galaxies is comparable in both environments, and (2) the supergroup's IR luminosity function has a higher L^*_{IR} than that previously measured for the field.

Key words: galaxies: clusters: general – galaxies: clusters: individual (SG1120-1202) – galaxies: evolution – galaxies: luminosity function, mass function – galaxies: starburst – infrared: galaxies

Online-only material: color figures

1. INTRODUCTION

Galaxies in the field environment span a wide range in morphology, color, and ongoing star formation (e.g., Marzke et al. 1998). In contrast, the significantly more crowded environment of galaxy clusters is dominated by passive, red, early-type galaxies that formed the bulk of their stars at $z > 2$ (Gregory & Thompson 1978; Dressler 1980; Bower et al. 1992; van Dokkum et al. 1998a). Using spectroscopically defined samples, several studies show that galaxies in clusters differ from their field counterparts even up to $z \sim 1.4$ (e.g., Holden et al. 2007; Mei et al. 2009; Lidman et al. 2008).

However, we know that the galaxy populations in clusters have evolved since at least $z \sim 1$. Observational examples of how the galaxy mix in clusters evolves with increasing redshift include: the increasing fraction of blue/star-forming members (Butcher & Oemler 1978; Ellingson et al. 2001), the increasing fraction of spectroscopically confirmed 24 μm sources (Saintonge et al. 2008, Paper I), the increasing fraction of massive post-starburst members (Tran et al. 2003; Poggianti et al. 2004), the increasing fraction of active galactic nuclei (Eastman et al. 2007; Kocevski et al. 2009), the increasing fraction of star-forming galaxies with increasing galaxy density at $z \sim 1$, a reversal of what is observed at $z \sim 0$ (Elbaz et al. 2007; Cooper et al. 2008), the decreasing fraction of S0 galaxies (Postman et al. 2005; Moran et al. 2007), and the decreasing fraction of faint red galaxies ($z > 0.5$; Tanaka et al. 2007; Stott et al. 2007; De Lucia et al. 2007, cf. Crawford et al. 2009).

[9] Based on observations made with (1) The ESO telescopes at Paranal Observatories under program IDs 072.A-0367, 076.B-0362, 078.B-0409; (2) the NASA/ESA *Hubble Space Telescope* (GO-10499); STScI is operated by the association of Universities for Research in Astronomy, Inc. under the NASA contract NAS 5-26555; (3) the *Spitzer Space Telescope*, which is operated by the Jet Propulsion Laboratory, California Institute of Technology under a contract with NASA; support for this work was provided by NASA through an award issued by JPL/Caltech (GO-20683); (4) the Chandra X-ray Observatory Center, which is operated by the Smithsonian Astrophysical Observatory for and on behalf of the National Aeronautics Space Administration under contract NAS8-03060; and (5) the Magellan 6.5 m telescope operated by OCIW.

The problem is that we have yet to identify clearly the physical mechanisms responsible for the dramatically different galaxy populations in clusters versus the field, nor the timescales needed for these mechanisms to operate. Although a plethora of physical processes have been invoked to quench star formation and transform galaxies into spheroidal systems, e.g., starvation (Bekki et al. 2002), ram-pressure stripping (Abadi et al. 1999), and galaxy harassment (Moore et al. 1998), stringent observational tests of when star formation is quenched and whether quenching is coupled to morphological transformation are needed to assess the relative importance of the physics at work. Simulations are sufficiently advanced that new insight can be obtained by, e.g., comparing star formation and gas-loss rates as a function of local density to the observations (Tonnesen et al. 2007).

Also, instead of focusing on massive clusters, the key to understanding the interplay between galaxy evolution and environment is to study galaxy groups because: (1) most galaxies in the local universe are in groups (e.g., Geller & Huchra 1983); and (2) hierarchical structure formation predicts that galaxy clusters assemble from the merger and accretion of smaller structures, e.g., groups (Peebles 1970). Simulations show that the physical mechanisms normally associated with galaxy clusters are also effective in groups (Hester 2006; Kawata & Mulchaey 2008; McCarthy et al. 2008), but that they operate in groups at lower redshifts (Romeo et al. 2008).

In fact, the galaxy groups in the local universe do have more in common with galaxy clusters than with the field population, i.e., higher early-type fractions and lower mean star formation rates than the field (Zabludoff & Mulchaey 1998; Hashimoto et al. 1998; Tran et al. 2001; Blanton & Berlind 2007; Rasmussen et al. 2008). With the advent of large spectroscopic studies such as Canadian Network for Observation Cosmology (CNOC; Yee et al. 1996) and Sloan Digital Sky Survey (SDSS; Abazajian et al. 2003), the galaxy populations in groups can now be studied for statistically large samples (e.g., Yang et al. 2007), and at intermediate redshifts (e.g., Poggianti et al. 2008; Gal et al. 2008; Knobel et al. 2009). Although still nascent, spectroscopic studies of galaxy groups at $z > 0.3$ find that the groups already have high early-type fractions (Jeltema et al. 2007; Wilman et al. 2008). However, whether star formation in $z > 0.3$ groups is enhanced or simply quenched relative to the field is debated (Poggianti et al. 2009; Balogh et al. 2009).

The question then is whether the evolution of galaxies in clusters is driven primarily on group or on cluster scales. Our discovery of a supergroup of galaxies at $z = 0.37$ allows us to uniquely answer this question. The supergroup (hereafter SG1120) is composed of multiple galaxy groups that we have shown will merge into a cluster comparable in mass to Coma by $z \sim 0$ (Gonzalez et al. 2005), unlike the majority of clusters studied at $z > 0.3$ that are too massive to be Coma progenitors. Because we know the galaxies in SG1120 will evolve into a cluster population, we can test whether the group galaxies are already like those in clusters. First results from our multi-wavelength study of SG1120 show that the group galaxies are in transition: SG1120 has a high fraction of early-type members (Kautsch et al. 2008), yet several of the most massive group galaxies are growing by dissipationless merging at $z < 0.4$ (Tran et al. 2008).

Here we focus on the dust-obscured star formation in the supergroup as measured with MIPS (Rieke et al. 2004) 24 μm observations. Studies find a surprising number of mid-infrared sources at cluster and group densities at $z > 0.3$ (Elbaz et al. 2007; Bai et al. 2007; Koyama et al. 2008; Dressler et al. 2009), but this may be due to the general increase in the fraction of mid-infrared galaxies with redshift (Le Floc'h et al. 2005). To determine if there is an excess of IR sources in the galaxy groups making up SG1120, we compare the 24 μm members in SG1120 to their counterparts in both the field and cluster environment at the same redshift.

For the cluster environment, we use CL 1358+62, a massive, dynamically evolved, X-ray luminous galaxy cluster at $z = 0.328$ with a line-of-sight velocity dispersion of 1027^{+51}_{-45} km s^{-1} (Fisher et al. 1998, hereafter F98). Most of the 232 spectroscopically confirmed members are passive, early-type galaxies (van Dokkum et al. 1998b). In addition to the spectroscopy, we have *HST*/WFPC2 mosaics taken in F606W and F814W covering $\sim 50\square'$, and MIPS 24 μm imaging.

The field sample is drawn from extensive observations of two higher redshift clusters: MS 2053−04 ($z = 0.59$; Tran et al. 2005) and MS 1054−03 ($z = 0.83$; Tran et al. 2007). In the combined area of approximately $50\square'$, we have measured spectroscopic redshifts for nearly 300 field galaxies at $0.09 < z < 1.36$. These fields were also imaged with *HST*/WFPC2 in F606W and F814W, and with MIPS at 24 μm. The depth and uniformity of our spectroscopic and photometric observations in these fields makes for a unique data set that enables robust comparison across environment at $z \sim 0.35$.

Our study of how 24 μm galaxies vary across environment is Paper II in our SMIRCS (*Spitzer*/MIPS Infra-Red Cluster Survey) series and complements Paper I (Saintonge et al. 2008) where we explored how the 24 μm fraction increases with increasing redshift in massive galaxy clusters at ($0 < z < 0.83$; see also R. Finn et al. 2009, in preparation). Throughout the paper, we use $H_0 = 70$ km s^{-1} Mpc^{-1}, $\Omega_M = 0.3$, and $\Omega_\Lambda = 0.7$; at $z = 0.37$, this corresponds to a scale of 5.12 kpc arcsec^{-1} and a look-back time of 4 Gyr. All rest-frame magnitudes are in the Vega system.

2. OBSERVATIONS

At these redshifts ($z \sim 0.35$), our large number of spectroscopically confirmed group (174) and cluster members (232) combined with multi-wavelength imaging that includes MIPS observations is unique among existing surveys. Unlike many spectroscopic cluster surveys at intermediate redshifts, we do not select by optical color which can bias a sample toward members that are already on the red sequence, e.g., against blue, star-forming members. The depth of our redshift surveys in the cluster fields also enables us to identify a sample of field galaxies ($0.25 \leqslant z \leqslant 0.45$; $\bar{z} = 0.35$) that have been observed and analyzed in the same manner as the group and cluster galaxies. The uniformity of our observations allows us to compare directly galaxy populations across a range of environments at $z \sim 0.35$.

2.1. Optical Imaging

2.1.1. Supergroup 1120 ($z \sim 0.37$)

The four X-ray luminous galaxy groups in the supergroup 1120-12 (hereafter SG1120) extend across an approximately $8' \times 12'$ region (Figure 1). Optical photometry of the group galaxies is measured from VLT/VIMOS (LeFevre et al. 2003) mosaics in BVR ($18' \times 20'$; $(\mathrm{PSF})_R \sim 0\farcs5$), Magellan/LDSS3 mosaics in $g'r'$ ($12' \times 20'$; $(\mathrm{PSF})_{r'} \sim 1\farcs0$), and a 10 pointing mosaic taken with *Hubble Space Telescope*/Advanced Camera for Surveys (*HST*/ACS) in F814W ($11' \times 18'$; $0\farcs05$/pixel). Near-infrared imaging was also

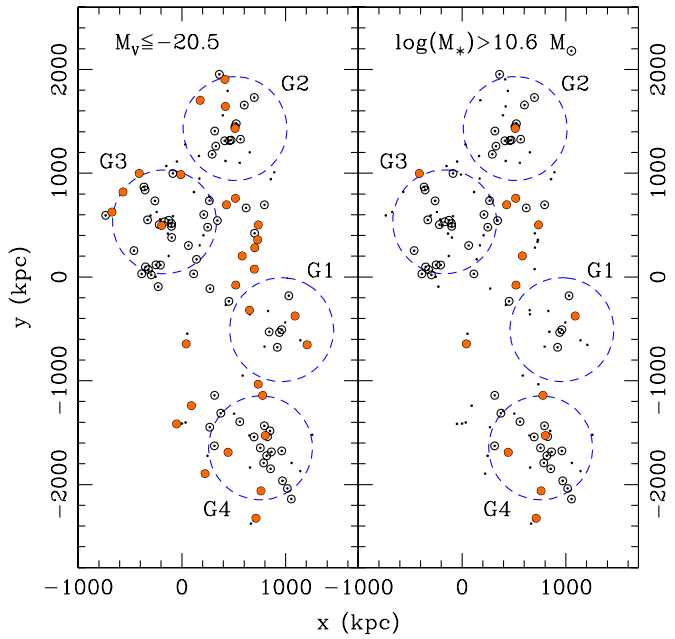

Figure 1. Spatial distribution of the spectroscopically confirmed supergroup galaxies that fall on the *HST*/ACS mosaic (small dots; $0.34 \leqslant z \leqslant 0.38$; 143 of 174 total members); north is up and east to the left. Left: open circles denote all group galaxies brighter than $M_V = -20.5$, and large filled circles denote members brighter than $M_V = -20.5$ with $\mathrm{SFR_{IR}} \geqslant 3\,M_\odot\ \mathrm{yr}^{-1}$. The large dashed circles ($R = 0.5\ h^{-1}$Mpc) are centered on the brightest group galaxies listed in Table 1; these positions are well matched to the extended X-ray emission detected in each group. Right: The same but for the mass-selected ($M_* > 4 \times 10^{10}\,M_\odot$) supergroup members. Note the number of luminous, 24 μm members outside the group cores that are low-mass systems ($10.0 < \log(M_*)[M_\odot] < 10.6$).

(A color version of this figure is available in the online journal.)

obtained with KPNO/FLAMINGOS[10] and provides a K_s mosaic ($16' \times 19'$; PSF $\sim 1''.2$). The wide-field mosaics are generated with *scamp* and *swarp*[11] (Bertin et al. 2002; Bertin 2006) which corrects the astrometry across the wide field and stitches the pointings together.

Line-matched photometric catalogs were generated using the VIMOS R mosaic as the master detection image (SExtractor v2.5.0; Bertin & Arnouts 1996). While several close galaxy pairs (separation $< 1''$) are considered single objects in the R catalog, this is appropriate for our analysis given that the same close pairs are also blended sources in the MIPS catalog (see Section 2.4). We use k-correct v4.1 (Blanton & Roweis 2007) to determine rest-frame absolute magnitudes (Vega) and K-corrections. As input, we use the MAG_AUTO photometry from the $g'BVr'R$ imaging and assumed minimum photometric uncertainties in each bandpass of 0.05 mag. The photometry has been corrected for foreground Galactic extinction using the Schlegel et al. (1998) dust maps and the O'Donnell (1994) Milky Way extinction curve, assuming $R_V = 3.1$.

For consistency and to thus ensure that our comparisons are robust across the supergroup, cluster, and field samples, we calculate stellar masses in the same manner by following the prescription in Bell et al. (2003). Here mass-to-light ratios $(M_*/L)_B$ are calculated from $(B - V)$ colors using

$$\log(M_*/L)_B = 1.737(B - V) - 0.942 \quad (1)$$

and a diet Salpeter initial mass function (IMF) is assumed. We use the diet Salpeter IMF defined in Bell & de Jong (2001) as having $x = 0$ below $0.6\,M_\odot$ and so the stellar mass using a diet Salpeter IMF is 70% of that for a regular Salpeter IMF (Salpeter 1955). Using an absolute magnitude for the Sun of $M_B = 5.45$[12], a galaxy with $M_B = -19.5$ and $(B - V) = 1$ has a stellar mass of $\log(M_*)[M_\odot] = 10.8$.

2.1.2. CL 1358+62 ($z = 0.328$)

The galaxy populations in CL 1358+62 ($z = 0.328$; F98) have been studied extensively using optical imaging and spectroscopy. For the cluster galaxies, we use the optical photometry measured by Holden et al. (2007, hereafter H07) from the *HST*/WFPC2 mosaics (total area of $\sim 50\square'$). To summarize, a Sérsic profile ($1 \leqslant n \leqslant 4$) was fit to the surface brightness distribution in the *HST*/WFPC2 imaging of each spectroscopically confirmed member; over 85% of the cluster members have $n \geqslant 2$. Galaxy colors were determined from fluxes measured within a half-light radius; the half-light radii were determined using the F814W imaging. Note that at $z \sim 0.33$, the redshifted B and V filters are well-matched to F606W and F814W. As in SG1120, we convert the observed fluxes (corrected for Galactic extinction) to rest-frame BV magnitudes using k-correct, and estimate stellar masses using Equation (1). For more details about the photometry and testing the robustness of the stellar mass determination for the cluster galaxies, we direct the reader to the extensive discussion in H07.

2.1.3. Field Galaxies ($\bar{z} = 0.35$)

Our field sample is drawn from a larger program that focused on galaxies in X-ray luminous clusters at intermediate redshifts. To select field galaxies in the same redshift range as SG1120 and CL1358, we use observations of galaxy clusters MS 2053–04 ($z = 0.59$; Tran et al. 2005) and MS1054–03 ($z = 0.83$; Tran et al. 2007). Both galaxy clusters were imaged by HST/WFPC2 in the F606W and F814W filters; each image mosaic is composed of six overlapping pointings and each mosaic covers an area of $\sim 25\square'$. The image reduction and photometry are detailed for MS2053 and MS1054 in Hoekstra et al. (2002) and van Dokkum et al. (2000), respectively.

Photometric catalogs were generated using SExtractor (see Tran et al. 2004) and we used k-correct to convert observed fluxes (measured with MAG_AUTO and corrected for Galactic extinction) to rest-frame BV magnitudes. As in the cases of the supergroup and cluster galaxies, stellar masses for the field galaxies are estimated using Equation (1).

2.2. Optical Spectroscopy

2.2.1. Supergroup 1120 ($0.34 < z < 0.38$)

The spectroscopic survey of the SG1120 field was completed using VLT/VIMOS (in 2003), Magellan/LDSS3 (in 2006), and VLT/FORS2 (in 2007; Appenzeller et al. 1998). The medium resolution spectroscopy corresponds to 2.5 Å pix^{-1} (VIMOS), 0.7 Å pix^{-1} (LDSS3), and 1.65 Å pix^{-1} (FORS2). Targets for the VIMOS masks were selected using $R \leqslant 22.5$ mag, and targets for the later runs selected using $K_s \leqslant 20$ mag. A

[10] FLAMINGOS was designed and constructed by the IR instrumentation group (PI: R. Elston) at the University of Florida, Department of Astronomy, with support from NSF grant AST97-31180 and Kitt Peak National Observatory.

[11] http://astromatic.iap.fr

[12] http://www.ucolick.org/~cnaw/sun.html

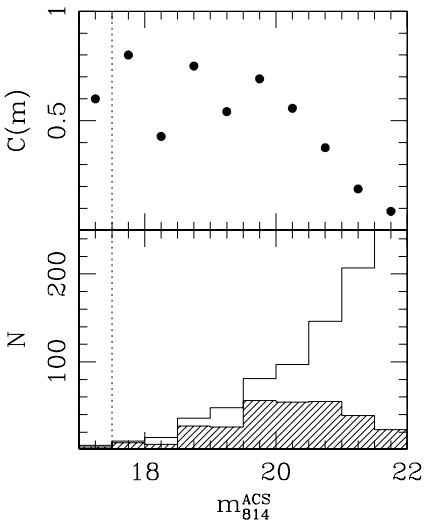

Figure 2. Top: for the SG1120 region, the spectroscopic completeness in the *HST*/ACS mosaic shown as a function of F814W magnitude; the dotted vertical line denotes the magnitude of the brightest group galaxy ($m_{814}^{ACS} = 17.5$). Bottom: histograms showing the total number of galaxies in the *HST*/ACS field (open), and those with redshifts (shaded). Variations in $C(m)$ at magnitudes brighter than 18.5 are due to small numbers (< 5) in each magnitude bin. The spectroscopic survey is $> 50\%$ complete at $m_{814}^{ACS} < 20.5$; our adopted magnitude limit of $M_V = -20.5$ mag corresponds approximately to $m_{814}^{ACS} = 20.4$.

total of 16 slit masks were observed at varying position angles; thus, our spectroscopic completeness is not affected by slit collisions.

Spectra from all of the observing runs were reduced using a combination of IRAF[13] routines and custom software provided by Kelson et al. (2000); see Tran et al. (2005) for further details on the spectral reductions. Redshifts were determined using IRAF cross-correlation routines, and each assigned redshift was visually compared to the one-dimensional spectrum. Each redshift was then given a quality flag where $Q = 3, 2, \&1$ corresponded to definite, probable, and maybe (single emission line). The spectral range for most of the supergroup members covers [O II]λ3727 to [O III]λ5007.

The spectroscopic completeness in the *HST*/ACS footprint is shown in Figure 2. Due to the supergroup's elongated structure (see Figure 1), spectra for a few of the bright ($m_{814}^{ACS} < 18.5$) galaxies have not been obtained; however, these are foreground galaxies. The brightest group galaxy has $m_{814}^{ACS} = 17.5$ mag, and the survey remains $> 50\%$ complete to $m_{814}^{ACS} = 20.5$ mag. For red supergroup members, the adopted magnitude limit used in our analysis of $M_V = -20.5$ mag (see Section 2.2.2) corresponds to $m_{814}^{ACS} = 20.4$ mag.

In the larger $20' \times 20'$ region centered on the *HST*/ACS mosaic, we have obtained spectra of 603 unique objects. Guided by breaks in the redshift distribution, we define group members to be at $0.34 \leqslant z \leqslant 0.38$ (Figure 3). Considering only galaxies with redshift quality flag of $Q = 3$ gives 174 supergroup members. Four of the five X-ray luminous regions correspond to galaxy groups at $0.35 < z < 0.37$, while the fifth is a galaxy cluster at $z = 0.48$ (Gonzalez et al. 2005). The coordinates, mean redshifts, and line-of-sight velocity dispersions of the individual groups are listed in Table 1, and Figure 1 shows the spatial distribution of members on the *HST*/ACS mosaic.

[13] IRAF is distributed by the National Optical Astronomy Observatories.

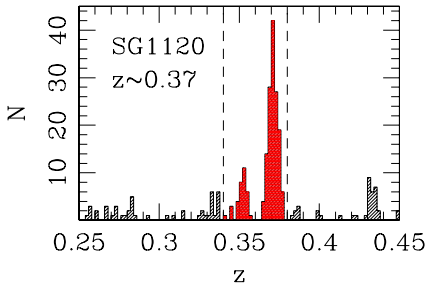

Figure 3. Redshift distribution of galaxies in the supergroup (SG1120) field; the redshift range for group members ($0.34 \leqslant z \leqslant 0.38$) is denoted by the vertical dashed lines. The brightest group galaxies lie at $0.354 \leqslant z \leqslant 0.372$.
(A color version of this figure is available in the online journal.)

Table 1
Properties of Galaxy Groups In SG1120.

ID	$(\alpha, \delta)^a$	$\bar{z}^b$	$\sigma_{1D}{}^b$	$N_g{}^b$	$T_X{}^c$
G1	(11:20:07.48, −12:05:09.1)	0.3522 ± 0.0008	303 ± 60	13	2.2
G2	(11:20:13.33, −11:58:50.6)	0.3707 ± 0.0007	406 ± 83	21	1.7
G3	(11:20:22.19, −12:01:46.1)	0.3712 ± 0.0005	580 ± 100	35	1.8
G4	(11:20:10.14, −12:08:51.6)	0.3694 ± 0.0005	567 ± 119	22	3.0

Notes.
[a] Coordinates (J2000) of the brightest galaxy in each group.
[b] Mean redshift ($\bar{z}$) and line-of-sight velocity dispersion (σ_{1D}; km s^{-1}) determined using galaxies (N_g) within 500 kpc of the brightest group galaxy; $\bar{z}$ and σ_{1D} are determined using the biweight and jackknife estimators (Beers et al. 1990), respectively.
[c] X-ray temperatures (keV) from Gonzalez et al. (2005).

2.2.2. CL 1358+62 ($0.315 < z < 0.342$)

A complete description of the spectroscopic survey in CL1358 including target selection, spectral reduction, wavelength calibration, sky subtraction, etc., is presented by F98. To summarize, WHT and MMT spectroscopy targeted objects with $R \leqslant 21$ mag over a $10' \times 11'$ region; at this magnitude limit, the spectroscopic survey is $> 80\%$ complete and not dependent on color (see F98, Figure 2). The magnitude limit corresponds approximately to $M_V = -20.5$, and we use this limit for our luminosity-selected samples. For reference, the Coma cluster has $M_V^* = -20.6$[14]

From nearly 400 redshifts, cluster membership was confirmed for 232 galaxies; in our analysis, we consider only the 171 members that fall on the *HST*/WFPC2 mosaic (total area of $\sim 50\square'$) that were studied by H07.

2.2.3. Field Galaxies ($0.25 \leqslant z \leqslant 0.45$)

As part of our program on galaxy clusters at intermediate redshift, we also obtained redshifts for a large sample of field galaxies. Spectroscopic targets were selected using a magnitude cut of $m_{814}^{WFPC2} \leqslant 23$ and $m_{814}^{WFPC2} \leqslant 23.5$ in the MS2053 and MS1054 fields, respectively. These magnitude-limited spectroscopic surveys were completed with Keck/LRIS (Oke et al. 1995) and resulted in a total of over 800 redshifts in the two fields; excluding the cluster members and considering only redshifts with $Q = 3$ provides 295 field galaxies at $0.09 < z < 1.36$. Further observational details for each field are in Tran et al. (2004). Notably, the spectroscopic completeness in both cluster fields is $> 80\%$ at $m_{814}^{WFPC2} < 21$ (see Figures 2 in Tran et al. 2005, 2007).

[14] Here we use $m_V^* = 14.5$ (Abell 1977) and a distance modulus of $(m - M) = 35.11$ (Baum et al. 1997) for the Coma cluster.

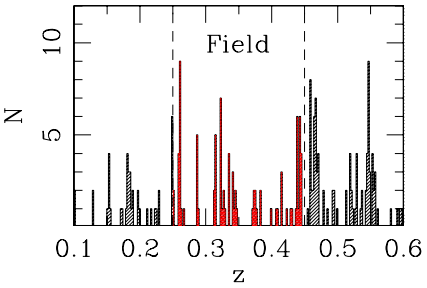

Figure 4. Redshift distribution of the field galaxies at $0.1 < z < 0.6$. These field galaxies are drawn from extensive spectroscopic surveys of two galaxy clusters, both of which are at $z > 0.55$. The redshift bins are $\Delta z = 0.002$ and are 5–10 times larger than the typical error in the redshift; any apparent overdensities disappear with smaller bin sizes. The vertical dashed lines denote the redshift range of our comparison field sample ($0.25 \leqslant z \leqslant 0.45$).

(A color version of this figure is available in the online journal.)

To ensure that we are observing the field galaxies at the same epoch as the group and cluster galaxies, we use only the field galaxies at $0.25 \leqslant z \leqslant 0.45$ ($\bar{z} = 0.35$; Figure 4). In this redshift range, we have 87 field galaxies; applying a magnitude ($M_V < -20.5$) or mass ($M_* \geqslant 4 \times 10^{10}\ M_\odot$) selection decreases the field sample to 28 and 21 galaxies, respectively (see Table 2). Note that both galaxy clusters MS2053 ($z = 0.59$; Tran et al. 2005) and MS1054 ($z = 0.83$; Tran et al. 2007) are at higher redshift, thus our field sample is not contaminated with cluster galaxies.

2.3. Hubble Type

We have visually classified Hubble types that were assigned using *HST* imaging for > 90% (371/401) of the spectroscopically defined galaxy sample across all three environments; at $M_V < -20.5$, an even higher fraction (97%; 225/232) of the galaxies are classified. The high-resolution *HST* imaging allows us to easily separate bulge versus disk-dominated galaxies, and even to distinguish between elliptical and S0s (Postman et al. 2005). We use a simplified Hubble scheme where T-types are assigned to elliptical ($-5 \leqslant T \leqslant -3$), S0 ($-2 \leqslant T \leqslant 0$), spiral+irregular ($1 \leqslant T \leqslant 10$), and merging ($T = 99$) galaxies.

In SG1120, we use the T-types assigned by Kautsch et al. (2008) to 142 of the 143 group galaxies that fall on the *HST*/ACS mosaic. The galaxy groups in SG1120 have velocity dispersions that are significantly lower than in massive clusters such as CL1358 (303–580 km s^{-1} versus 1027 km s^{-1}; see Table 1), yet the groups are already dominated by early-type members: SG1120's early-type fraction of $\sim$ 70% is already comparable to that of galaxy clusters at intermediate redshifts (Kautsch et al. 2008).

For the cluster (CL1358) and field galaxies, we have T-types assigned by D. Fabricant, M. Franx, and P. van Dokkum using *HST*/WFPC2 imaging (Fabricant et al. 2000). This team classified all galaxies in the cluster fields brighter than $m_{814}^{\rm WFPC2} = 22$; these classifications have been published in vD98, van Dokkum et al. (2000), and Tran et al. (2005). From this database, 161 of the 171 CL1358 galaxies in H07's sample and 67 of the 87 field galaxies ($0.25 \leqslant z \leqslant 0.45$) have visual classifications.

2.4. MIPS 24 μm Imaging

Deep wide-field 24 μm imaging of all the fields presented in our study was taken with MIPS (Rieke et al. 2004). We briefly summarize here the procedure for retrieving, reducing, and analyzing the MIPS imaging; further details are in Paper I. For SG1120, we retrieved the MIPS 24 μm data sets from the *Spitzer* archive and corrected the individual frames with the scan mirror position-dependent flats before combining the frames with the MOPEX software to a pixel size of 1.″2. The integration time per pixel was 1200 s and the background level 35.5 MJy sr^{-1}.

With the large SG1120 MIPS mosaic (22′ × 56′), we were able to determine a good point-spread function (PSF) and thus measure 24 μm fluxes via profile fitting. As a check, we compared the fluxes measured via profile fitting to aperture fluxes and found the values to be consistent; for the latter, we used an aperture diameter of 2″ as a compromise between maximizing the flux and minimizing contamination from close neighbors, and applied corrections based on fluxes derived from modeled PSFs (see Paper I). We matched the centroid position of the MIPS sources to the master *R*-band catalog. We estimated the completeness of the SG1120 24 μm catalog by adding 50 sources modeled on the empirical PSF to the mosaic and repeating this process 20 times.

To convert the 24 μm fluxes to star formation rates, we determined the total infrared (IR) luminosity ($F_{8-1000\mu{\rm m}}$) for each galaxy using a family of IR spectral energy distributions (SEDs) from Dale & Helou (2002). Using the range of SEDs that are representative of galaxies in the *Spitzer* Infrared Nearby Galaxies Survey (Dale et al. 2007), we adopt the median conversion factor from $F_{24\mu{\rm m}}$ to $F_{8-1000\mu{\rm m}}$ at $z \sim 0.37$ where the SEDs give essentially the same values and the error due to the adopted conversion factor is only $\sim$ 10%–20%. Combining

Table 2
MIPS 24 μm Galaxy Fractions.

Selection	Number	Field	Group	Cluster
All[a]	N	87	143	171
Luminosity-selected Samples				
$M_V < -20.5$	N	29	98	105
	$N_{\rm IR}$	11	31	7
	IR%	37.9%	31.6%	6.7%
$M_V < -20.5$ Late-types[b]	N	18	37	21
	$N_{\rm IR}$	11	27	7
	IR%	61.1%	73.0%	33.3%
$M_V < -20.5$ Early-types[b]	N	8	61	80
	$N_{\rm IR}$	0	4	0
	IR%	0.0%	6.6%	0.0%
Mass-selected Samples				
$\log(M_*)[M_\odot] > 10.6$	N	22	72	103
	$N_{\rm IR}$	8	14	5
	IR%	36.4%	19.4%	4.9%
$\log(M_*)[M_\odot] > 10.6$ Late-types[b]	N	12	16	18
	$N_{\rm IR}$	8	11	5
	IR%	66.7%	68.8%	27.8%
$\log(M_*)[M_\odot] > 10.6$ Early-types[b]	N	8	56	81
	$N_{\rm IR}$	0	3	0
	IR%	0.0%	5.3%	0.0%

Notes.
[a] Considering only spectroscopically confirmed members that fall on the *HST* imaging.
[b] Late-type (disk-dominated) galaxies have Hubble classification of $T > 0$ and early-type (bulge-dominated) galaxies have $T \leqslant 0$.

this conversion with the completeness simulations, we estimate that the SG1120 24 μm catalog is 80% complete to $\log(L_{\rm IR})$[erg s^{-1}] = 43.8; this corresponds to a 24 μm flux of approximately 105μJy and an IR star formation rate of SFR$_{\rm IR} \geqslant 3\,M_\odot$ yr^{-1} (Rieke et al. 2009).

For the smaller cluster fields, we followed essentially the same procedure except that we used APEX to measure fluxes within a 2″ diameter aperture and corrected the measured fluxes using the PSF from the SG1120 mosaic. The total integration times and background levels in these mosaics vary, but the 24 μm imaging is essentially confusion-limited in these fields (see Paper I). We estimated the completeness of the 24 μm catalogs by adding 30 sources into each mosaic and repeated the process 20 times for each mosaic. The 24 μm catalogs are deeper than in the SG1120 field, e.g., the CL1358 24 μm catalog is 80% complete to $\log(L_{\rm IR})$[erg s^{-1}] = 43.5.

3. RESULTS

In the following analysis, we consider only the 143 supergroup galaxies in SG1120 that fall on the *HST*/ACS mosaic, the 171 cluster galaxies in CL1358 with photometry measured by H07 from the *HST*/WFPC2 mosaics, and the 87 field galaxies at $0.25 \leqslant z \leqslant 0.45$, all of which also have *HST*/WFPC2 imaging. We are thus assured of a uniformly selected sample and can directly compare results across the three environments.

Our 24 μm imaging identifies all galaxies with obscured star formation rates of 3 $M_\odot$ yr^{-1} or greater, regardless of galaxy mass. However, actively star-forming galaxies tend to have lower mass-to-light ratios than galaxies dominated by older stars, e.g., galaxies on the red sequence; thus, an optical luminosity-selected sample is likely to differ from a mass-selected sample. For this reason, we use both luminosity and mass-selected samples in our analysis to check the robustness of our results. Note that in fitting the infrared luminosity functions (IR LFs), we select based on total IR luminosity as determined with the 24 μm fluxes.

3.1. Fraction of 24 μm Sources

We first apply a luminosity limit set by the spectroscopic completeness in the CL1358 field (see Section 2.2) and consider only galaxies with absolute *V*-band (Vega) magnitude brighter than −20.5; due to the mixed galaxy population in our $z \sim 0.35$ samples, we do not correct for passive evolution. The color–magnitude (CM) diagram for the galaxies in all three environments is shown in Figure 5. The slope of the CM relation in each panel is from vD98 who measured the CM relation in CL1358 using the early-type members; the CM relation is normalized to the red sequence in CL1358. The color deviation from the CM relation is denoted as $\Delta(B-V)$ where blue galaxies are classically defined as having $\Delta(B-V) < -0.2$ (Butcher & Oemler 1978).

In the luminosity-limited sample, the fraction of 24 μm sources in the cluster is significantly lower than in the field ($7 \pm 2\%$[15] versus $36 \pm 9\%$; Table 2). However, we find that *the fraction of 24 μm sources in the supergroup ($32 \pm 5\%$) is comparable to the field and 4 times greater than in the cluster*. Figure 6 shows *HST*/ACS images of the supergroup galaxies with SFR$_{\rm IR} \geqslant 3\,M_\odot$ yr^{-1} and $M_V < -20.5$.

Because ongoing star formation can increase a galaxy's total optical luminosity and thus scatter lower mass systems into the luminosity-selected sample, we compare our results to a mass-selected sample (Table 2). As in Paper I, we consider only galaxies with stellar masses greater than $M_* = 4 \times 10^{10}\,M_\odot$. Again, the fraction of 24 μm sources in the supergroup is higher than in the cluster ($19\% \pm 5\%$ versus $5\% \pm 2\%$; Table 2); however, the fraction in the supergroup is now only about half that of the field.

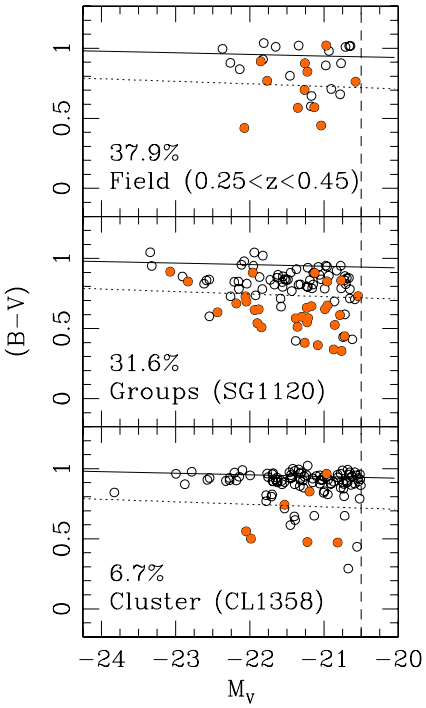

Figure 5. Rest-frame CM diagram of galaxies brighter than $M_V = -20.5$ (dashed vertical line) in the field (top), galaxy groups (middle), and galaxy cluster (bottom). The galaxies with SFR$_{\rm IR} \geqslant 3\,M_\odot$ yr^{-1} are shown as filled circles; the corresponding fractions are listed in each panel. The slope of the CM relation (solid line) is from vD98 and normalized to the red sequence in CL1358; the same CM relation is shown in each panel. The 24 μm fraction in the galaxy groups is nearly as high as in the field and is 4 times higher than in the cluster.

(A color version of this figure is available in the online journal.)

In applying a mass-cut, we discover that SG1120 has a significant number of members (17; see Figure 6) that are bright ($M_V < -20.5$), mostly late-type galaxies with stellar masses of ($10.0 < \log(M_*)[M_\odot] < 10.6$). Once star formation is quenched in these systems, they will fade and redden, and most will have $L < L^*$, i.e., they will populate the faint end of the red sequence.

We have assumed that the 24 μm emission is due to star formation but as many authors have noted (e.g., Donley et al. 2008), there is a likely contribution from dust-enshrouded active galactic nuclei (AGNs). However, we stress that AGN contamination does not impact our conclusions because the relative fraction in each environment is small. In a 70 ksec *Chandra*/ACIS image of the SG1120 field (Gonzalez et al. 2005), only four of the 143 group galaxies are detected as X-ray point sources. As for the cluster galaxies ($z = 0.33$), Martini et al. (2007) estimate that the AGN fraction in two $z \sim 0.3$ clusters is less than 3%. The possible number of the field AGN is equally low: using Donley et al.'s (2008) survey of IR-detected AGNs, we estimate that only one of the field IR sources can be an AGN. Note that if we account for these estimates of the AGN fraction, the difference in the IR star-forming fraction between

[15] Given the small number statistics, we assume a binomial distribution to calculate the error on the fractions.

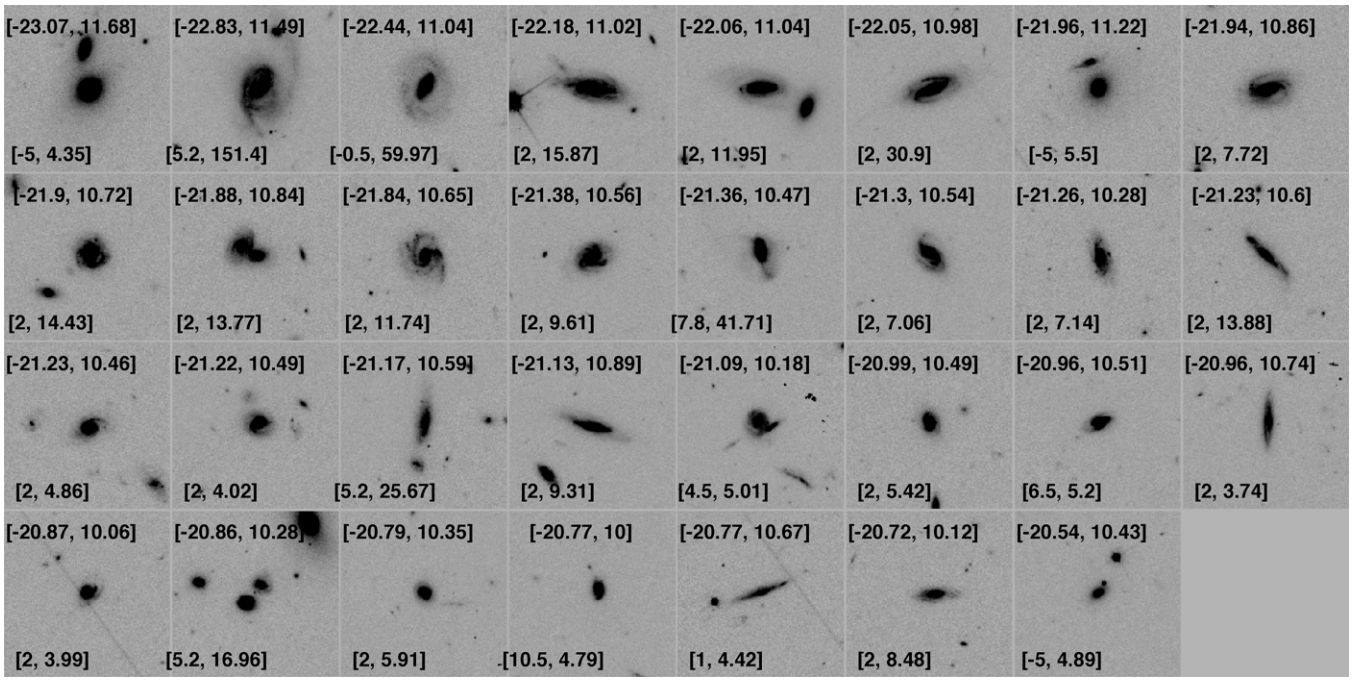

Figure 6. Images ($15'' \times 15''$) of the supergroup galaxies that fall on the *HST*/ACS mosaic ($M_V < -20.5$) with $\mathrm{SFR_{IR}} \geqslant 3\ M_\odot\ \mathrm{yr}^{-1}$. Each image lists the absolute V magnitude (Vega) and estimated $\log(M_*)[M_\odot]$ on top, as well as the galaxy's *Hubble* Type and 24 μm SFR on the bottom. Close galaxy pairs (separation $< 1''$) are considered single objects in both the master R catalog and MIPS catalog (see Section 2.1 & Section 2.4) because of the 24 μm imaging's resolution (resampled pixel scale of $1''.2$).

the supergroup and cluster environment only increases ($\sim 28\%$ versus $\sim 4\%$ in the luminosity-selected samples).

3.2. Infrared Luminosity Function

To better quantify how the 24 μm sources in the supergroup differ from their counterparts in the cluster and in the field, we compare the IR LFs of the supergroup (SG1120) and cluster (CL1358) with published results from the field in Figure 7. We correct the observations in both SG1120 and CL1358 for spectroscopic and 24 μm incompleteness; the 80% completeness limit for the 24 μm sources is $\log(L_{\mathrm{IR}})[\mathrm{erg\ s^{-1}}]$= 43.8 and 43.5 in the supergroup and galaxy cluster, respectively.

To fit the IR distribution, we follow Bai et al. (2006) and first use a Schechter function (Schechter 1976):

$$\phi(L) = \phi^* \left(\frac{L}{L^*}\right)^{-\alpha} \exp^{(-L/L^*)}, \quad (2)$$

where we fix the faint-end slope α, and adopt the best-fit chi-square minimization method to determine L^* and ϕ^* (Table 3). Because studies show the IR LF in general has a relatively large number of bright sources and is better described by a double-exponential function (Le Floc'h et al. 2005), we adopt their approach and also fit a double-exponential function:

$$\phi(L) = \phi^* \left(\frac{L}{L^*}\right)^{(1-\alpha)} \exp\left\{-\left(\frac{1}{2\sigma^2}\right)\log^2\left[1+\left(\frac{L}{L^*}\right)\right]\right\}, \quad (3)$$

where we fix the constants α and σ to the values measured for the field IR LF, and minimize with chi-square again. Note that to determine the faint-end slope α in either function, deeper IR observations are required (Bai et al. 2006).

The IR LFs in both the supergroup and galaxy cluster are well fit by both a Schechter and a double-exponential function

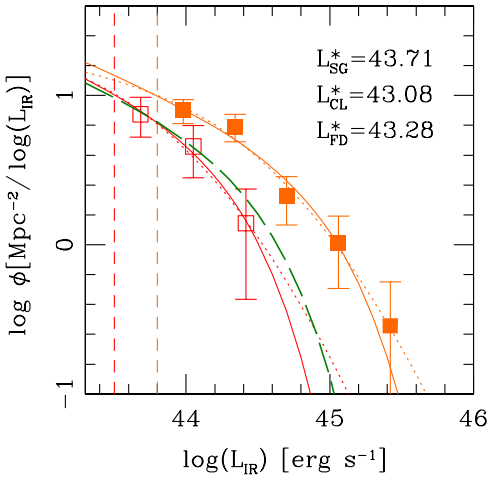

Figure 7. IR LFs of the galaxy groups ($z \sim 0.37$; solid squares) and the galaxy cluster ($z = 0.33$; open squares); 1σ error bars are included. The vertical dashed lines at $\log(L_{\mathrm{IR}})[\mathrm{erg\ s^{-1}}]$= 43.8 and 43.5 correspond to the 80% completeness limit of the 24 μm sources for the galaxy groups and the cluster, respectively. The IR LFs in both environments are well fit by both Schechter (solid curves) and double-exponential (dotted curves) functions. The IR LF of the cluster galaxies is consistent with the IR LF of $z \sim 0$ clusters evolved to $z \sim 0.35$ (long-dashed curve; see the text for details), but the group IR LF has an excess of sources.

(A color version of this figure is available in the online journal.)

(Figure 7) using different values for L^* and ϕ^* (see Table 3). However, the density of IR sources in the supergroup is dramatically higher than in the cluster, especially at $\log(L_{\mathrm{IR}})$ $[\mathrm{erg\ s^{-1}}] > 45$.

Perhaps the large difference is due to CL1358 being unusually deficient in IR sources. We test this by taking the IR LF determined from 24 μm observations of galaxy clusters at $z \sim 0$ (Bai et al. 2006) and evolve the IR LF to $z \sim 0.35$ using the observed evolution in the field IR LF (Le Floc'h et al. 2005).

Table 3
Infrared Luminosity Function Parameters.

Function	Environment	$\log(L^*_{\rm IR})$	$\phi^*_{\rm IR}$
Schechter[a]	Group	$44.99^{+0.19}_{-0.19}$	$3.4^{+1.4}_{-0.9}$
Schechter[a]	Cluster	$44.33^{+0.32}_{-0.25}$	$5.3^{+4.0}_{-3.5}$
Schechter[a]	Evolved[b]	44.53	4.0
Double-exponential[c]	Group	$43.71^{+0.19}_{-0.19}$	$11.8^{+4.7}_{-3.2}$
Double-exponential[c]	Cluster	$43.08^{+0.37}_{0.46}$	$17.4^{+32.2}_{-8.8}$
Double-exponential[c]	(Field)[d]	$43.28^{+0.09}_{0.03}$	...

Notes.
[a] For the Schechter profile, we set $\alpha_{\rm IR} = 1.414$ (Bai et al. 2006, 2007).
[b] IR LF measured in $z \sim 0$ galaxy clusters (Bai et al. 2006) evolved to $z \sim 0.35$ using the evolution measured in the field IR LF (Le Floc'h et al. 2005).
[c] For the double-exponential profile, we set $\alpha_{\rm IR} = 1.23$ and $\sigma_{\rm IR} = 0.72$ (Le Floc'h et al. 2005)
[d] Field $L^*_{\rm IR}$ measured by Le Floc'h et al. (2005) for galaxies at $(0.3 < z < 0.45)$; we do not include $\phi^*_{\rm IR}$ because it is normalized differently in the field and in clusters.

Bai et al. (2007, 2009) find that $L^*_{\rm IR}$ and $\phi^*_{\rm IR}$, as derived from 24 μm observations, evolve in approximately the same manner in galaxy clusters and the field to $z \sim 0.8$, although see Muzzin et al. (2008) for an alternative result. The IR LF for CL1358 ($z = 0.33$) is consistent with the evolved cluster IR LF (Figure 7; long-dashed curve). However, the density of IR sources in the supergroup is ~ 10 times higher than the number predicted from the evolved IR LF at $\log(L_{\rm IR})[{\rm erg\ s^{-1}}] > 45$.

The IR LF in the supergroup also differs from the IR LF for the field measured by Le Floc'h et al. (2005). The best-fit double-exponential function to the group IR LF has a measurably larger $L^*_{\rm IR}$ compared to the value for field galaxies at $(0.3 < z < 0.45)$: $43.71^{+0.19}_{-0.19}$ versus $43.28^{+0.09}_{-0.03}$. In comparison, Bai et al. (2009) find a similar $L^*_{\rm IR}$ value for both local cluster and field galaxies. (Table 3). SG1120's higher $L^*_{\rm IR}$ relative to even that measured for the field suggests that star formation is enhanced in the group environment.

To summarize, the number of IR sources in the galaxy groups that make up SG1120 is significantly higher than in CL1358, a rich galaxy cluster at $z = 0.33$, and includes a population of very bright IR sources ($\log(L_{\rm IR})[{\rm erg\ s^{-1}}] > 45$) that are not found in CL1358 nor in lower redshift clusters. The higher value of $\log(L^*_{\rm IR})$ in the supergroup compared to that measured for the field at $(0.3 < z < 0.45)$ also indicates that the IR sources in the supergroup differ from their counterparts in the field, i.e., that star formation likely is enhanced in the group environment.

3.3. Local Environment

Having established that the 24 μm population in the supergroup (SG1120) is different from that in the cluster (CL1358) and likely also the field environment, we examine how the galaxy populations for the luminosity-selected samples ($M_V < -20.5$) depend on local environment, i.e., how star formation rate relates to galaxy density (Balogh et al. 1998; Gómez et al. 2003). In addition to the IR-bright population, we separate galaxies into optically defined absorption-line ([O II]λ3727 $<$ 5 Å) and emission-line ([O II]λ3727 $\geqslant$ 5 Å) systems. In the supergroup and cluster, we define the local galaxy density Σ using the distance to the 10th nearest spectroscopically confirmed neighbor; we note that the following results do not change if we use instead the 5th nearest neighbor.

Figure 8 (top left) shows how the fraction of ${\rm SFR_{IR}} \geqslant 3\ M_\odot\ {\rm yr^{-1}}$ members in the supergroup steadily increases with decreasing local density. The increasing fraction of emission-line members with decreasing Σ mirrors the trend for IR members, and the absorption-line fraction changes accordingly. The trend of an increasing IR fraction with decreasing local density remains even if we apply higher IR star formation rate threshold of $5\ M_\odot\ {\rm yr^{-1}}$. In contrast, the IR population in the cluster (top right) shows essentially no trend with local environment: the absorption-line population dominates throughout the range of local densities explored here ($5 < \Sigma < 70$ gal Mpc^{-2})[16]. These results are in line with Paper I where we also find an increase in 24 μm members outside the cores of massive clusters ($R_{\rm proj} > 700\ h^{-1}$kpc). Our results argue for a physical mechanism that quenches star formation before the members reach the group cores.

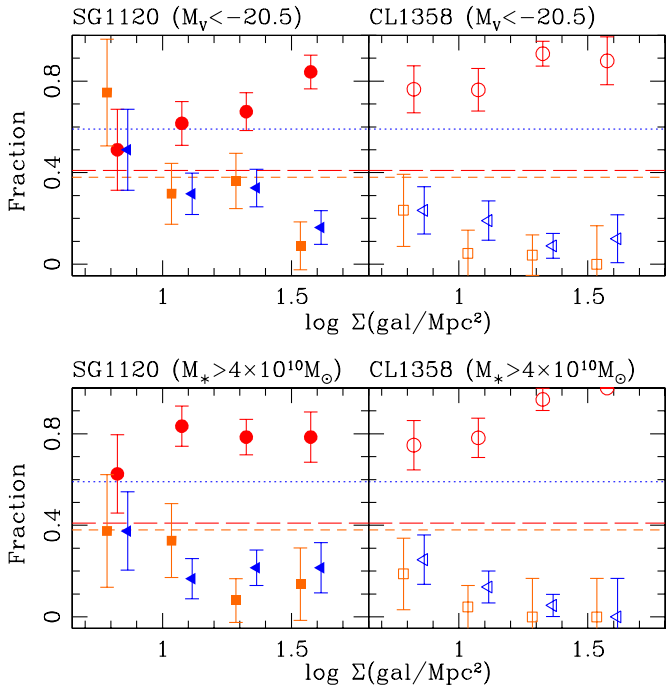

Figure 8. Relative fraction of absorption-line (circles), emission-line (triangles), and 24 μm (squares) members as a function of local galaxy surface density in the groups (SG1120, left panels, filled symbols) and cluster (CL1358, right panels, open symbols); the points are offset slightly in $\log\Sigma$ for clarity. The top panels show the luminosity-selected ($M_V < -20.5$) members and the bottom panels the mass-selected ($M_* > 4 \times 10^{10}\ M_\odot$) members. The long-dashed, dotted, and short-dashed horizontal lines show, respectively, the absorption-line, emission-line, and 24 μm fractions in the field. Only in the supergroup with a luminosity-selected sample does the 24 μm fraction increase steadily with decreasing local density, i.e., an IR star formation–density relation.
(A color version of this figure is available in the online journal.)

At the lowest galaxy densities, the fraction of IR members in the supergroup is higher than even in the field: considering all members with $\Sigma < 20$ gal Mpc^{-2}, the IR fraction increases to 49% (26/53) compared to the field value of 38% (Table 2). At these low galaxy densities, the higher fraction of IR members in the supergroup relative to the field, while statistically not significant, is consistent with the higher $L^*_{\rm IR}$ measured in the group environment (see Table 3).

If we now examine how the mass-selected ($M_* > 4 \times 10^{10}\ M_\odot$) samples depend on local environment (Figure 8, bottom panels), the trend of increasing 24 μm fraction with decreasing galaxy density in the supergroup is weaker: the

[16] While the galaxy density in the cluster environment extends to $\Sigma > 100$ gal Mpc^{-2}, we consider only the Σ range that overlaps with the galaxy groups.

absorption-line population dominates in both the group and the cluster environment at $\Sigma > 10$ gal Mpc^{-2}. These results are consistent with H07 who find that evolution in the early-type fraction in massive clusters ($0 < z < 0.8$) is weaker when considering only galaxies with $M_* > 4 \times 10^{10}\,M_\odot$versus a luminosity-selected sample, thus galaxies with lower masses play a significant role in the observed evolution of the cluster galaxy population.

We find that the supergroup has a population of luminous, 24 μm detected late-type members with stellar masses of ($10.0 < \log(M_*)[M_\odot] < 10.6$) that are mostly outside the groups' cores (see Figures 1 and 6), i.e., at lower galaxy densities. It is these galaxies that cause the strong observed trend of decreasing 24 μm fraction with increasing galaxy density in the *luminosity-selected* sample. As noted in Section 3.1, most of these will fade and redden and can populate the faint end of the red sequence once their star formation is quenched.

4. DISCUSSION

To study how galaxies evolve, galaxies are usually separated into active/emission-line and passive/absorption-line systems with the goal of isolating the physical process that connects the two phases, e.g., removal of a galaxy's gas halts its star formation and the galaxy evolves from an active system into a passive one (Abadi et al. 1999; Kawata & Mulchaey 2008). The high fraction of 24 μm galaxies in the supergroup and the field means that obscured star formation (IR phase) is important for at least 30% of optically selected galaxies in both these environments; the IR phase is likely to be as important in clusters given that clusters grow via the accretion of field and group galaxies (Peebles 1970). In the following, we examine the physical properties of the 24 μm galaxies to better understand where the IR population fits into our current picture of galaxy evolution.

4.1. Morphologies of 24 μm Galaxies

To determine what the typical morphology of a 24 μm galaxy is across environment at $z \sim 0.35$, we separate the samples into late-type ($T > 0$; disk-dominated) and early-type ($T \leqslant 0$; bulge-dominated) systems. In both the field and supergroup, most ($> 60\%$) of the late-type galaxies are IR-detected; the supergroup even has a few bulge-dominated systems that are IR-detected[17]. In contrast, only $\sim 30\%$ of the late-type galaxies in the cluster are IR-detected, and none of the cluster's bulge-dominated members are IR-detected. These differences are true in both the luminosity- and mass-selected samples (Table 2).

Comparing the 24 μm galaxies in the supergroup to the field again strongly suggests a difference between the two environments. In the luminosity-selected samples, the supergroup and field have similar 24 μm fractions. However, the supergroup has a much higher fraction of E/S0 members: the E/S0 fraction in the supergroup is $\sim 60\%$ but it is only $\sim 30\%$ in the field[18] (Table 2). Several of the 24 μm galaxies in the supergroup are in merging, disk-dominated systems (see Figure 6), but only one of the massive dissipationless merging pairs (Tran et al. 2008) is detected at 24 μm.

Despite having double the fraction of early-type galaxies compared to the field, the supergroup has a high 24 μm fraction due to a population of luminous ($M_V < -20.5$), low-mass ($M_* < 4 \times 10^{10}\,M_\odot$) late-type members with SFR$_{\rm IR} \geqslant 3\,M_\odot$ yr^{-1} (see Section 3.1, Section 3.3, & Table 2). Note that in the mass-selected sample, the 24 μm fraction in the supergroup drops from $\sim 32\%$ to $\sim 19\%$, while the field fraction remains high ($\sim 35\%$). Our results show that the timescales for morphological evolution and quenching of star formation must differ (see also R. Finn et al. 2009, in preparation).

4.2. Star Formation on the Red Sequence

Across all three environments, there are 24 μm sources that are also on the optical red sequence (see Figure 5); here we use the classical definition of the red sequence as galaxies with $\Delta(B - V) > -0.2$ (Butcher & Oemler 1984). The fraction of red 24 μm sources depends on environment: it is highest in the field (21%; 6/29), decreases in the supergroup (7%; 7/98), and is lowest in the cluster (3%; 3/105). These results do not depend on whether we use the luminosity or mass-selected sample.

Our results appear to conflict with Gallazzi et al. (2009) who find that the fraction of red 24 μm sources in the Abell 901/902 supercluster ($z = 0.165$; Gray et al. 2002) peaks at intermediate densities typical of cluster outskirts and galaxy groups[19]. However, the authors estimate the field contamination in their magnitude range can be as high as 20%, and our study shows that the fraction of red 24 μm galaxies in the field is ~ 3 times higher than in the groups. By using a spectroscopically selected sample, we circumvent possible problems due to field contamination.

In A901/902, Wolf et al. (2009) find that the dusty red star-forming members are primarily spiral galaxies, and that this population mostly overlaps with the "optically passive" spirals (as defined by color). We find similar results: all of the red 24 μm galaxies in the field and cluster are disk-dominated systems ($T > 0$), and most of the red 24 μm galaxies ($\sim 60\%$) in the groups are spirals as well (see Figure 6).

We note that neither optical colors nor optical spectroscopy reliably identifies dusty red [$\Delta(B - V) > -0.2$] star-forming spirals: summing across environment, only (10/15) of the red 24 μm galaxies have [O II]λ3727 > 5 Å, i.e., one third of 24 μm members on the red sequence show no significant [O II] emission. This result is in line with earlier studies, e.g., Moustakas et al. (2006), that show optical spectroscopy can severely underestimate the level of activity. On a related note, many 24 μm galaxies can be strongly extincted with E(B-V) values as high as 0.6 (Cowie & Barger 2008); once corrected for extinction, many of the 24 μm galaxies would not lie on the red sequence.

4.3. Progenitors of Faint Red Galaxies

As the groups in SG1120 merge to form a galaxy cluster, how do the 24 μm members impact the overall galaxy population? In Figure 9, we plot specific star formation rates (defined as SFR$_{\rm IR} \geqslant 3\,M_\odot$ yr^{-1} divided by stellar mass) versus stellar mass for the 24 μm galaxies in the supergroup, field, and cluster. Assuming the 24 μm members maintain their current star formation rates, perhaps only five out of the 72 massive

[17] While none of the eight early-types in the field have SFR$_{\rm IR} \geqslant 3\,M_\odot$ yr^{-1}, this is likely due to our relatively small field sample because Lotz et al. (2008) do find a number of early-type galaxies at ($0.4 < z < 1.2$) with comparable IR luminosities.

[18] The E/S0 fraction in our field sample is consistent with the E/S0 fraction measured by Driver et al. (1998) for a significantly larger field sample.

[19] Because Gallazzi et al. (2009) estimate local galaxy density differently, we cannot compare their values directly to Figure 8. These authors use a spectroscopic sample supplemented with members selected with photometric redshifts.

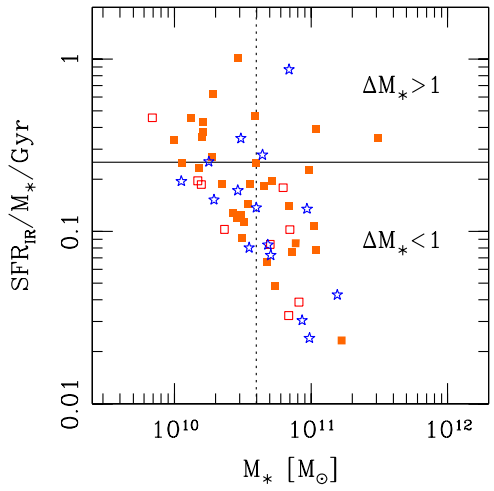

Figure 9. The 24 μm-derived specific star formation rate (SSFR) in units of Gyr for the galaxy groups (filled squares), cluster (open squares), and the field sample (stars); the dotted vertical line denotes $M_* = 4 \times 10^{10}\,M_\odot$ and we show only members with $\mathrm{SFR_{IR}} \geqslant 3\,M_\odot\ \mathrm{yr}^{-1}$. If we assume constant SFRs, the galaxies above the horizontal line will more than double their stellar mass from $z \sim 0.37$ to now. At most, perhaps four of the 72 massive galaxies in SG1120 can double their stellar mass. However, there are a number of lower mass ($10.0 < \log(M_*)[M_\odot] < 10.6$) group galaxies that can grow substantially in stellar mass (upper left quadrant); these are luminous late-type members with $\mathrm{SFR_{IR}} \geqslant 3\,M_\odot\ \mathrm{yr}^{-1}$.

(A color version of this figure is available in the online journal.)

($M_* > 4 \times 10^{10}\,M_\odot$) group galaxies will double their stellar masses, i.e., virtually all of the massive galaxies that will end up in the cluster are already in place.

In our analysis, we have identified a considerable number of luminous ($M_V < -20.5$) galaxies in the supergroup that have $\mathrm{SFR_{IR}} \geqslant 3\,M_\odot\ \mathrm{yr}^{-1}$ and stellar masses below $4 \times 10^{10}\,M_\odot$(17/98; Table 2); it is this population that contributes the most to the difference between the 24 μm population in the supergroup and in the cluster. Figure 9 shows that even if these group galaxies can maintain their current star formation rates, most (15/17; $\sim$ 90%) will still have stellar masses of $M_* < 10^{11}\,M_\odot$ at $z \sim 0$; the current average stellar mass for all 17 galaxies is $\log(M_*)[M_\odot] = 10.4$. Note that most of these members are at $R_{\mathrm{proj}} > 0.5$ Mpc from their respective group cores (see Figure 1).

We test our hypothesis that these galaxies can evolve into ($L < L^*$) red galaxies by comparing their stellar masses to the faint red galaxies in CL1358, our massive galaxy cluster. Following De Lucia et al. (2007), we define faint red galaxies as having luminosities of $(0.1 - 0.4)L^*$[20] and $\Delta(B - V) > -0.2$. The average stellar mass of the faint red galaxies in the cluster is $\log(M_*)[M_\odot] = 10.3$; this is comparable to the average stellar mass of the luminous, low-mass, $\mathrm{SFR_{IR}} \geqslant 3\,M_\odot\ \mathrm{yr}^{-1}$ supergroup galaxies. Assuming their star formation is quenched by $z \sim 0$, these supergroup galaxies will fade and redden to lie on the CM relation in less than a Gyr (see models by Bruzual & Charlot 2003). Their younger luminosity-weighted ages relative to the more massive galaxies will be consistent with the observed age spread in the Coma cluster (Poggianti et al. 2001). We stress that the luminous, low-mass, $\mathrm{SFR_{IR}} \geqslant 3\,M_\odot\ \mathrm{yr}^{-1}$ supergroup galaxies are likely to be only one of multiple progenitors of faint red galaxies.

[20] Using $M_V^* = -20.6$, the corresponding Vega V-band magnitudes are ($-20.1 < M_V < 19.6$).

5. SUMMARY

To quantify how dust-obscured star formation varies with environment, we compare galaxies in a super galaxy group to those in the field and in a massive cluster at $z \sim 0.35$ using a rich multi-wavelength data set that includes imaging from *Hubble* (optical), *Chandra* (X-ray), and *Spitzer* (24 μm). The strength of our work relies on extensive optical spectroscopy in our fields: the magnitude-limited spectroscopic surveys yielded a total of over 1800 unique redshifts and enable us to securely identify field, supergroup, and cluster members. We focus on the four X-ray luminous galaxy groups at $z \sim 0.37$ (SG1120-12) that will merge to form a galaxy cluster comparable in mass to Coma (Gonzalez et al. 2005); the groups have line-of-sight velocity dispersions of 303–580 km s^{-1}. To ensure robust comparison, we consider only field galaxies at $0.25 \leqslant z \leqslant 0.45$ ($\bar{z} = 0.35$) and confirmed members of the massive galaxy cluster CL1358+62 ($z = 0.33$, Fisher et al. 1998).

We find that the supergroup has a significantly higher fraction of dusty star-forming members than the massive galaxy cluster: in the luminosity-selected ($M_V < -20.5$) samples, 32% of the supergroup members have $\mathrm{SFR_{IR}} \geqslant 3\,M_\odot\ \mathrm{yr}^{-1}$ compared to only 7% of the cluster members. The supergroup's IR LF confirms that the density of IR sources is dramatically higher in the groups compared to the cluster. The supergroup members also include bright IR sources ($\log(L_{\mathrm{IR}})[\mathrm{erg\ s}^{-1}] > 45$) not found in galaxy clusters at $z \lesssim 0.35$.

When selected by luminosity, the supergroup members show a strong trend of decreasing 24 μm fraction with increasing local galaxy density, i.e., an IR–density relationship. This mirrors the trend in the optically active members (as defined by [O II] emission). In contrast, the fraction of 24 μm sources in the massive cluster stays essentially zero at all densities.

Comparison to the mass-selected ($M_* > 4 \times 10^{10}\,M_\odot$) samples reveals that the higher 24 μm fraction and the IR–density relation in the supergroup is due primarily to a population of luminous ($M_V < -20.5$), lower mass ($10.0 < \log(M_*)[M_\odot] < 10.6$), late-type members with $\mathrm{SFR_{IR}} \geqslant 3\,M_\odot\ \mathrm{yr}^{-1}$ ($\sim$ 17%). Most of these members are outside of the group cores ($R_{\mathrm{proj}} \geqslant 0.5$ Mpc). Assuming their star formation is quenched in the next $\sim$ 3–4 Gyr, these members will fade and redden by $z \sim 0$, and most will become fainter ($L < L^*$) galaxies on the color-magnitude relation. The physical mechanism that quenches their star formation must be effective outside the group cores, i.e., in lower density environments.

In the supergroup, the excess of 24 μm sources, the number of very bright 24 μm members, and the IR–density relationship is surprising because the E/S0 fraction is already as high as in the cluster (> 60% for luminosity-selected sample; Kautsch et al. 2008). No further morphological evolution is required to bring the morphological distribution of the groups in line with the high early-type fractions observed in local galaxy clusters. In other words, the timescale for morphological transformation must not be strongly coupled to when star formation is completely quenched.

Our analysis indicates that the 24 μm population in the supergroup differs even from the field: 1) the supergroup's IR luminosity function has a measurably higher L^*_{IR} than the field; and 2) the E/S0 fraction in the supergroup is twice that of the field, yet the 24 μm fraction in both environments are comparable. If dusty star formation is enhanced in the supergroup relative to the field, our IR–density analysis suggests that it occurs at densities of $\Sigma < 20$ gal Mpc^{-2}. A larger field

sample selected with the same criteria as in the supergroup and cluster is needed to answer this question securely.

Our study highlights the importance of understanding galaxy evolution on group scales. A significant fraction ($\gtrsim$ 30%) of optically selected galaxies in both the supergroup and field at $z \sim 0.35$ have dust-obscured star formation; the IR phase must be as important in clusters because clusters grow by accreting galaxy groups and field galaxies. As demonstrated in recent simulations of galaxy groups (e.g., Hester 2006; Romeo et al. 2008; McCarthy et al. 2008; Kawata & Mulchaey 2008), the physical mechanisms that affect star formation and induce morphological evolution are already well underway in the galaxy groups that make up SG1120. We will continue dissecting how these galaxies are transformed by using recently obtained IFU observations to map the kinematics and star formation of the 24 μm members.

K.T. and A.S. acknowledge support from the Swiss National Science Foundation (grant PP002-110576). J.M. acknowledges support from NASA-06-GALEX06-0030 and *Spitzer* G05-AR-50443, and L.B. from NASA *Spitzer* programs through JPL subcontracts Nos. 1255094 and 1256318. Support was also provided by NASA *HST* G0-10499, JPL/Caltech SST GO-20683, and Chandra GO2-3183X3.

Facilities: VLT (VIMOS), VLT (FORS2), Magellen (LDSS3), KPNO (Mayall 4m), *HST* (ACS), *SST* (MIPS), CXO (ACIS), Keck (LRIS).

REFERENCES

Abadi, M. G., Moore, B., & Bower, R. G. 1999, MNRAS, 308, 947
Abazajian, K., et al. 2003, AJ, 126, 2081
Abell, G. O. 1977, ApJ, 213, 327
Appenzeller, I., et al. 1998, The Messenger, 94, 1
Bai, L., Rieke, G. H., Rieke, M. J., Christlein, D., & Zabludoff, A. I. 2009, ApJ, 693, 1840
Bai, L., Rieke, G. H., Rieke, M. J., Hinz, J. L., Kelly, D. M., & Blaylock, M. 2006, ApJ, 639, 827
Bai, L., et al. 2007, ApJ, 664, 181
Balogh, M. L., et al. 2009, MNRAS, 398, 754
Balogh, M. L., Schade, D., Morris, S. L., Yee, H. K. C., Carlberg, R. G., & Ellingson, E. 1998, ApJ, 504, L75
Baum, W. A., Hammergren, M., Thomsen, B., Groth, E. J., Faber, S. M., Grillmair, C. J., & Ajhar, E. A. 1997, AJ, 113, 1483
Beers, T. C., Flynn, K., & Gebhardt, K. 1990, AJ, 100, 32
Bekki, K., Couch, W. J., & Shioya, Y. 2002, ApJ, 577, 651
Bell, E. F., & de Jong, R. S. 2001, ApJ, 550, 212
Bell, E. F., McIntosh, D. H., Katz, N., & Weinberg, M. D. 2003, ApJS, 149, 289
Bertin, E. 2006, in ASP Conf. Ser. 351, Astronomical Data Analysis Software and Systems XV, ed. C. Gabriel, C. Arviset, D. Ponz, & S. Enrique (San Francisco, CA: ASP), 112
Bertin, E., & Arnouts, S. 1996, A&AS, 117, 393
Bertin, E., Mellier, Y., Radovich, M., Missonnier, G., Didelon, P., & Morin, B. 2002, in ASP Conf. Ser. 281, Astronomical Data Analysis Software and Systems XI, ed. D. A. Bohlender, D. Durand, & T. H. Handley (San Francisco, CA: ASP), 228
Blanton, M. R., & Berlind, A. A. 2007, ApJ, 664, 791
Blanton, M. R., & Roweis, S. 2007, AJ, 133, 734
Bower, R. G., Lucey, J. R., & Ellis, R. S. 1992, MNRAS, 254, 601
Butcher, H., & Oemler, A. 1978, ApJ, 219, 18
Butcher, H., & Oemler, A. 1984, ApJ, 285, 426
Bruzual, G., & Charlot, S. 2003, MNRAS, 344, 1000
Cooper, M. C., et al. 2008, MNRAS, 383, 1058
Cowie, L. L., & Barger, A. J. 2008, ApJ, 686, 72
Crawford, S. M., Bershady, M. A., & Hoessel, J. G. 2009, ApJ, 690, 1158
Dale, D. A., & Helou, G. 2002, ApJ, 576, 159
Dale, D. A., et al. 2007, ApJ, 655, 863
De Lucia, G., et al. 2007, MNRAS, 374, 809
Donley, J. L., Rieke, G. H., Pérez-González, P. G., & Barro, G. 2008, ApJ, 687, 111
Dressler, A. 1980, ApJ, 236, 351
Dressler, A., Rigby, J., Oemler, A., Fritz, J., Poggianti, B. M., Rieke, G., & Bai, L. 2009, ApJ, 693, 140
Driver, S. P., Fernandez-Soto, A., Couch, W. J., Odewahn, S. C., Windhorst, R. A., Phillips, S., Lanzetta, K., & Yahil, A. 1998, ApJ, 496, L93
Eastman, J., Martini, P., Sivakoff, G., Kelson, D. D., Mulchaey, J. S., & Tran, K.-V. 2007, ApJ, 664, L9
Elbaz, D., et al. 2007, A&A, 468, 33
Ellingson, E., Lin, H., Yee, H. K. C., & Carlberg, R. G. 2001, ApJ, 547, 609
Fabricant, D., Franx, M., & van Dokkum, P. 2000, ApJ, 539, 577
Fisher, D., Fabricant, D., Franx, M., & van Dokkum, P. 1998, ApJ, 498, 195
Gal, R. R., Lemaux, B. C., Lubin, L. M., Kocevski, D., & Squires, G. K. 2008, ApJ, 684, 933
Gallazzi, A., et al. 2009, ApJ, 690, 1883
Geller, M. J., & Huchra, J. P. 1983, ApJS, 52, 61
Gómez, P. L., et al. 2003, ApJ, 584, 210
Gonzalez, A. H., Tran, K. H., Conbere, M. N., & Zaritsky, D. 2005, ApJ, 624, L73
Gray, M. E., Taylor, A. N., Meisenheimer, K., Dye, S., Wolf, C., & Thommes, E. 2002, ApJ, 568, 141
Gregory, S. A., & Thompson, L. A. 1978, ApJ, 222, 784
Hashimoto, Y., Oemler, A. J., Lin, H., & Tucker, D. L. 1998, ApJ, 499, 589
Hester, J. A. 2006, ApJ, 647, 910
Hoekstra, H., Franx, M., Kuijken, K., & van Dokkum, P. G. 2002, MNRAS, 333, 911
Holden, B. P., et al. 2007, ApJ, 670, 190
Jeltema, T. E., Mulchaey, J. S., Lubin, L. M., & Fassnacht, C. D. 2007, ApJ, 658, 865
Kautsch, S. J., Gonzalez, A. H., Soto, C. A., Tran, K.-V. H., Zaritsky, D., & Moustakas, J. 2008, ApJ, 688, L5
Kawata, D., & Mulchaey, J. S. 2008, ApJ, 672, L103
Kelson, D. D., Illingworth, G. D., van Dokkum, P. G., & Franx, M. 2000, ApJ, 531, 159
Knobel, C., et al. 2009, ApJ, 697, 1842
Kocevski, D. D., Lubin, L. M., Gal, R., Lemaux, B. C., Fassnacht, C. D., & Squires, G. K. 2009, ApJ, 690, 295
Koyama, Y., et al. 2008, MNRAS, 391, 1758
LeFevre, O., et al. 2003, Proc. SPIE, 4841, 1670
Le Floc'h, E., et al. 2005, ApJ, 632, 169
Lidman, C., et al. 2008, A&A, 489, 981
Lotz, J. M., et al. 2008, ApJ, 672, 177
Martini, P., Mulchaey, J. S., & Kelson, D. D. 2007, ApJ, 664, 761
Marzke, R. O., da Costa, L. N., Pellegrini, P. S., Willmer, C. N. A., & Geller, M. J. 1998, ApJ, 503, 617
McCarthy, I. G., Frenk, C. S., Font, A. S., Lacey, C. G., Bower, R. G., Mitchell, N. L., Balogh, M. L., & Theuns, T. 2008, MNRAS, 383, 593
Mei, S., et al. 2009, ApJ, 690, 42
Moore, B., Lake, G., & Katz, N. 1998, ApJ, 495, 139
Moran, S. M., Loh, B. L., Ellis, R. S., Treu, T., Bundy, K., & MacArthur, L. A. 2007, ApJ, 665, 1067
Moustakas, J., Kennicutt, R. C., Jr., & Tremonti, C. A. 2006, ApJ, 642, 775
Muzzin, A., Wilson, G., Lacy, M., Yee, H. K. C., & Stanford, S. A. 2008, ApJ, 686, 966
O'Donnell, J. E. 1994, ApJ, 422, 158
Oke, J. B., et al. 1995, PASP, 107, 375
Peebles, P. J. E. 1970, AJ, 75, 13
Poggianti, B. M., Bridges, T. J., Komiyama, Y., Yagi, M., Carter, D., Mobasher, B., Okamura, S., & Kashikawa, N. 2004, ApJ, 601, 197
Poggianti, B. M., et al. 2001, ApJ, 563, 118
Poggianti, B. M., et al. 2008, ApJ, 684, 888
Poggianti, B. M., et al. 2009, ApJ, 693, 112
Postman, M. et al. 2005, ApJ, 623, 721
Rasmussen, J., Ponman, T. J., Verdes-Montenegro, L., Yun, M. S., & Borthakur, S. 2008, MNRAS, 388, 1245
Rieke, G. H., Alonso-Herrero, A., Weiner, B. J., Pérez-González, P. G., Blaylock, M., Donley, J. L., & Marcillac, D. 2009, ApJ, 692, 556
Rieke, G. H., et al. 2004, ApJS, 154, 25
Romeo, A. D., Napolitano, N. R., Covone, G., Sommer-Larsen, J., Antonuccio-Delogu, V., & Capaccioli, M. 2008, MNRAS, 389, 13
Saintonge, A., Tran, K.-V. H., & Holden, B. P. 2008, ApJ, 685, L113 (Paper I)
Salpeter, E. E. 1955, ApJ, 121, 161
Schechter, P. 1976, ApJ, 203, 297
Schlegel, D. J., Finkbeiner, D. P., & Davis, M. 1998, ApJ, 500, 525
Stott, J. P., Smail, I., Edge, A. C., Ebeling, H., Smith, G. P., Kneib, J.-P., & Pimbblet, K. A. 2007, ApJ, 661, 95
Tanaka, M., Kodama, T., Kajisawa, M., Bower, R., Demarco, R., Finoguenov, A., Lidman, C., & Rosati, P. 2007, MNRAS, 377, 1206

Tonnesen, S., Bryan, G. L., & van Gorkom, J. H. 2007, ApJ, 671, 1434
Tran, K. H., Franx, M., Illingworth, G., Kelson, D. D., & van Dokkum, P. 2003, ApJ, 599, 865
Tran, K. H., Franx, M., Illingworth, G. D., van Dokkum, P., Kelson, D. D., & Magee, D. 2004, ApJ, 609, 683
Tran, K. H., Simard, L., Zabludoff, A. I., & Mulchaey, J. S. 2001, ApJ, 549, 172
Tran, K. H., van Dokkum, P., Illingworth, G. D., Kelson, D., Gonzalez, A., & Franx, M. 2005, ApJ, 619, 134
Tran, K.-V. H., Franx, M., Illingworth, G. D., van Dokkum, P., Kelson, D. D., Blakeslee, J. P., & Postman, M. 2007, ApJ, 661, 750
Tran, K.-V. H., Moustakas, J., Gonzalez, A. H., Bai, L., Zaritsky, D., & Kautsch, S. J. 2008, ApJ, 683, L17
van Dokkum, P. G., Franx, M., Fabricant, D., Illingworth, G. D., & Kelson, D. D. 2000, ApJ, 541, 95
van Dokkum, P. G., Franx, M., Kelson, D. D., & Illingworth, G. D. 1998a, ApJ, 504, L17
van Dokkum, P. G., Franx, M., Kelson, D. D., Illingworth, G. D., Fisher, D., & Fabricant, D. 1998b, ApJ, 500, 714
Wilman, D. J., et al. 2008, ApJ, 680, 1009
Wolf, C., et al. 2009, MNRAS, 393, 1302
Yang, X., Mo, H. J., van den Bosch, F. C., Pasquali, A., Li, C., & Barden, M. 2007, ApJ, 671, 153
Yee, H. K. C., Ellingson, E., & Carlberg, R. G. 1996, ApJS, 102, 269
Zabludoff, A. I., & Mulchaey, J. S. 1998, ApJ, 496, 39